REPORT DOCUMENTATION PAGE

Public reporting burden for this collection of information is estimated to average 1 hour per response, including the time for reviewing instructions, searching existing data sources, gathering and maintaining the data needed, and completing and reviewing this collection of information. Send comments regarding this burden estimate or any other aspect of this collection of information, including suggestions for reducing this burden to Department of Defense, Washington Headquarters Services, Directorate for Information Operations and Reports (0704-0188), 1215 Jefferson Davis Highway, Suite 1204, Arlington, VA 22202-4302. Respondents should be aware that notwithstanding any other provision of law, no person shall be subject to any penalty for failing to comply with a collection of information if it does not display a currently valid OMB control number. **PLEASE DO NOT RETURN YOUR FORM TO THE ABOVE ADDRESS.**

1. REPORT DATE (DD-MM-YYYY)	2. REPORT TYPE		3. DATES COVERED (From - To)
	Technical Paper		

4. TITLE AND SUBTITLE	5a. CONTRACT NUMBER
Please see attached	5b. GRANT NUMBER
	5c. PROGRAM ELEMENT NUMBER

6. AUTHOR(S)	5d. PROJECT NUMBER
	2308
	5e. TASK NUMBER
	M13C
	5f. WORK UNIT NUMBER
	346057

7. PERFORMING ORGANIZATION NAME(S) AND ADDRESS(ES)	8. PERFORMING ORGANIZATION REPORT
ERC	

9. SPONSORING / MONITORING AGENCY NAME(S) AND ADDRESS(ES)	10. SPONSOR/MONITOR'S ACRONYM(S)
Air Force Research Laboratory (AFMC) AFRL/PRS 5 Pollux Drive Edwards AFB CA 93524-7048	11. SPONSOR/MONITOR'S NUMBER(S) *Please see attached*

12. DISTRIBUTION / AVAILABILITY STATEMENT

Approved for public release; distribution unlimited.

13. SUPPLEMENTARY NOTES

14. ABSTRACT

20030116 064

15. SUBJECT TERMS

16. SECURITY CLASSIFICATION OF:			17. LIMITATION OF ABSTRACT	18. NUMBER OF PAGES	19a. NAME OF RESPONSIBLE PERSON Leilani Richardson
a. REPORT	b. ABSTRACT	c. THIS PAGE	A		19b. TELEPHONE NUMBER (include area code)
Unclassified	Unclassified	Unclassified			(661) 275-5015

Visual Characteristics and Initial Growth Rates of Round Cryogenic Jets at Subcritical and Supercritical Pressures

.B. Chehroudi[*], D. Talley[†], and E. Coy[†]

*Engineering Research Corporation
AFRL/PRSA
10 E. Saturn Boulevard
Edwards AFB, CA 93524-7680
(corresponding author)

[†]Air Force Research Laboratory
AFRL/PRSA
10 E. Saturn Boulevard
Edwards AFB, CA 93524-7680
661-275-6175

Short Abstract

The visual characteristics and initial growth rates of round cryogenic jets injected into subcritical and supercritical pressures were studied. It was found that the jet exhibits liquid-like and gas-like characteristics at subcritical and supercritical pressures, respectively. Explanations are offered. The jet spreading angle at supercritical pressures has been demonstrated to agree quantitatively with the theoretical spreading angle of incompressible but variable density turbulent gas jets, the first time more than a qualitative visual similarity with gas jets has ever been demonstrated. In addition, the present measurements of spreading rates have been plotted along with other measurements for subsonic incompressible constant density and variable density jets, liquid sprays, supersonic jets, and other mixing layers in a plot spanning four orders of magnitude in gas-to-liquid density ratio. This is the first time these results have been consolidated in a single plot over such a large range of density ratio.

are (126.2, 3.4), (154.6, 5.04), and (32.94, 1.28), respectively. Very little information is available in the fluid physics literature on liquid jets injected into a supercritical environment, especially when the jets are cryogenic liquids. This motivated initiating an organized and systematic experimental investigation of initially liquid jets injected at sub- and supercritical pressures.

There are drastic changes in some important equilibrium properties of a pure substance as it approaches the thermodynamic critical point (CP). For example, under thermodynamic equilibrium condition[s] the sharp distinction between liquid and gas phases disappears at and above the critical pressure, and the substance is more properly considered to be a fluid whose density can vary widely but continuously as temperature is changed at fixed pressure. Density changes can become particularly large near the critical point. Other properties that vary widely near the critical point are the thermal conductivity and mass diffusivity. In addition, the constant-pressure specific heat becomes very large and surface tension vanishes. Finally, the solubility of gases into the liquid phase becomes significant as the ambient pressure is raised, making it necessary to consider multicomponent phase equilibrium or nonequilibrium.[1] For mixtures, the determination of critical conditions, called the "critical mixing temperature or pressure" (critical lines for a two-component mixture as opposed to a critical point for a pure substance), can be complex.[2] For example, for a pure hydrocarbon drop in a nitrogen environment, the amount of nitrogen dissolved on the surface of the liquid drop increases with pressure.[3] As a result, the critical mixing temperature of the layer decreases.[4] This forms a layer which is a mixture of nitrogen and fuel that spreads spatially in time. In what follows, unless otherwise made clear, the terms subcritical and supercritical, and the reduced pressure and temperature, will refer to the critical condition of the pure substance used in the drops or jets and not that of the mixture.

There are only a few studies of liquid injection into supercritical conditions.[5-9] *Newman and Brzustowski*[5] studied steady CO_2 jets injected into a chamber of pure N_2 and also mixtures of CO_2+N_2 at both sub- and supercritical pressures and temperatures. They explained the effects of increased chamber temperature on the jet appearance to be due to the progressive reduction in ambient gas density, the reduction in surface tension to zero at the critical temperature, and the increase in liquid CO_2 evaporation. Based on coarse photographs, they proposed the possibility of jet gasification, namely that at supercritical temperatures and pressures the jet could be treated as a variable density single phase turbulent submerged gas jet. *Mayer, et. al.,*[6] studied liquid cryogenic N_2 (LN$_2$) jets at a fixed temperature of 105 K injected into a N_2 environment at 300 K, but at varying ambient sub- to supercritical pressures, and observed drastic changes in the jet structure near and above the critical pressure. They attributed this behavior to a continual decline of surface tension until it vanished at and above the critical pressure. They also studied the coaxial injection of LN$_2$ (at 97 K) inside gaseous He (at 280 K), as simulant fluids for H_2 and O_2, the coaxial configuration being similar to ones used in cryogenic rocket engines. As before, changes in the jet structure as pressure increases were clearly observed, and attributed to increases in the solubility of He into N_2 and reductions in the surface tension. Finally, they studied H_2 / O_2 combustion in a windowed model rocket combustion chamber, and again observed structural changes in the jet with pressure in both the ignition and steady state combustion phases. No evidence of droplets was observed at supercritical conditions. *Woodward and Talley*[9] studied the injection of LN$_2$ jets into gaseous N_2 and gaseous mixtures of N_2 and He at much lower Reynolds numbers than the above studies. For N_2/N_2 systems, observation of the resulting fluid structures at and above the critical pressure showed strong evidence that surface tension becomes negligibly small either at the instant of mass injection or very rapidly thereafter. Adding gaseous He (~20 wt%), however, was found to produce structures which again showed strong evidence of having surface tension at pressures up to twice the critical pressure of pure N_2, demonstrating the strong effect of composition on the critical mixing properties.

about 5.5 mm (axial distance/diameter ratio of 21.6) from the injector and hence buoyancy effects can be ignored in favor of the inertial forces.

Figure 2 shows images of a cold (90–110 K) N_2 jet injected into warm N_2 at a fixed supercritical chamber temperature (300 K) but at various pressures ranging above and below the critical pressure. Objects of 30 +/- 7 microns and larger can be resolved in these images. The reduced pressures $P_r = P_{chamber} / P_{critical}$ shown are given with respect to the critical pressure of pure nitrogen. The images show a demarcation of regions where changes in index of refraction occur due to density variations. At the lowest subcritical chamber pressure in Fig. 2, P_r=0.23, the jet is liquid-like with surface instabilities that grow downstream, where it has twisted appearance. At P_r=0.43, all instabilities are further amplified, until at P_r=0.63, many surface ligaments and drops are seen to be ejected from the jet. At P_r=0.83, very fine drops are seen surrounding the jet and its spanwise dimension noticeably grows away from the injector exit plane (i.e., the jet diverges). At P_r=1.03 the N_2 jet enters into a supercritical temperature and pressure environment. There are drastic changes in the details of the interface. There are no detectable drops under this condition with the highest software magnification used to view these high resolution images. There are thread- or finger-like entities emerging from the jet which are not broken up into droplets as before but are seemingly dissolved at a spectrum of distances from the dark core. This, in a sense, forms a mixing layer in which phase transition and/or large local density nonuniformities occur. Any further increase of the chamber pressure decreases the length and the thickness of the internal dark core, and images progressively resemble the injection of a gaseous turbulent jet into a gaseous environment.

Figure 3 shows selected images from Fig. 2 under additional magnification. The images are chosen to represent typical mixing layer regimes at subcritical, transitional, and supercritical pressures. At subcritical pressures, the gas-to-liquid density ratio is reasonably low, and jet behavior corresponds more or less to classical liquid atomization theory. The left hand picture in Fig. 3 corresponds roughly to second wind-induced jet breakup regime (see further discussion below). At higher pressures near the critical pressure, the jet enters into a transitional regime where coherent comb-like dense structures are dissipated into the surroundings about as fast as they can be ejected by turbulence from the jet. Droplets are no longer formed, but comb-like structures remain at the interface. As the pressure increases further above the critical pressure, the density ratio becomes increasingly larger, causing the aforementioned dense structures to disappear. The mixing layer increasingly resembles that of a classical gas/gas turbulent mixing layer. An examination of a large number of images at high magnification revealed no evidence of any droplet formation in this gas/gas regime. These observations are consistent with the observations of *Mayer, et. al.*[6] and *Newman and Brzustowski.*[5]

It is worthwhile to relate the images in Figs. 2 and 3 to classical liquid jet breakup regimes. Classical liquid jet breakup refers here to the condition at fixed gas-to-liquid density ratios having a fairly small magnitude (~.002). For a narrow range of density ratio, atomization and breakup regimes of liquid jets can be mapped onto plots of Ohnesorge number $Oh = \mu_l/(\rho_l \sigma d)^{1/2}$ versus Reynolds number $Re = \rho_l U d/\mu_l$, where U is liquid exit velocity , d is the nozzle diameter, and ρ_l, σ, and μ_l are the liquid density, surface tension, and viscosity, respectively. For a fixed fluid properties at a fixed exit nozzle diameter (i.e. fixed Ohnesorge number), increasing the exit velocity causes a horizontal path to be traced from left to right as the Reynolds number increases. According to *Reitz and Bracco,*[14] at small gas-to-liquid density ratios, liquid jet breakup regimes change along this horizontal path as the Reynolds number increases from Rayleigh liquid jet breakup, to the first and second wind-induced breakup, and finally to the liquid full atomization or simply atomization regime. Rayleigh breakup is caused by the growth of axisymmetric oscillations of the jet surface, induced by surface tension, and drop diameters larger than the jet diameter are

many small droplets, clearly indicative of second wind-induced atomization. The other is when the latter structure changes, not into full atomization, but into a gas/gas-like jet appearance near but below the critical pressure. The reason for the latter is due to the progressive reduction of surface tension and the enthalpy of vaporization approaching zero.

Similar observations were made for cryogenic O_2 injected into warm gaseous N_2. It was observed that similar transition characteristics occurred, but at a pressure nearer to the critical pressure for oxygen.

Jet growth rate

One important geometrical parameter that can be quantitatively evaluated in Fig. 2 is the initial jet spreading angle, or its growth rate. This parameter was measured for all acquired images and the results along with those of other researchers are presented in Fig. 4. The angles measured here are determined from the information within a 5.5 mm distance close to the injector exit face (distance-to-diameter ratio of up to 21.6). Note that according to *Abramovich*,[17] the length of the potential core in isothermal uniform density axisymmetric two dimensional jets are estimated to be about 6 to 10 injector diameters, whereas for nonisothermal cold jets injected into hot environments, the potential core can reach up to about 25 injector diameters, depending on the jet temperature. Also, according to *Chehroudi, et. al.*,[18] the intact core of liquid sprays similar to the ones used in diesel engines is given by $Cd(\rho_l/\rho_g)^{1/2}$, where ρ_l and ρ_g are liquid injectant and chamber gas densities, respectively, d is the effective jet exit diameter, and C is a constant between 3.3 to 11. This implies an intact core length of between 33 to 110 injector diameters for a chamber-to-injectant density ratio of 0.01, and 16.5 to 55 diameters for a density ratio of 0.04. As will be discussed further below, the density ratio range of 0.01 to 0.04 corresponds to the observed spray-like behavior of the jet. Thus the spreading rate data measured here within 5.5 mm of the injector face corresponds to the mixing layer region surrounding the potential core.

For each condition, 20 images were used to form an averaged image from which angle measurements are made for presentation in Fig. 4. Two angles are measured, namely, the angle determined by the outermost observable extent of the jet, commonly used for growth rate determination, and the angle determined by the extent of the spreading of the dark-looking internal core. The maximum uncertainty band on the angle measurements is shown for the O_2 and N_2 data in Fig. 4. The inverse procedure was also investigated. The angle for each of the 20 images per condition was measured separately, and then averaged. No appreciable differences were observed between the two procedures.

Of importance in Fig. 4 is the justification for the selection of the data sets and the nature of their measurements by other researchers. They are elaborated in the following. An adequate description and review of data by others is offered so that a deeper appreciation of Fig. 4 and its uniqueness can be realized with a reasonable degree of self-sufficiency. Since the jets investigated here exhibit both liquid-like and gas-like jet appearances, appropriate results for both are reviewed.

The simplest result is perhaps the prediction of the linear jet growth or constant spreading angle for a turbulent incompressible submerged jet. This is derived using the mixing length concept as detailed in the Appendix. Here, the parameter "2b", the jet thickness from the velocity profiles, is apparently measured at the 95% roll-off point. Next, following *Abramovich*[17], is the semi-empirical equation that attempts to incorporate the effects of density variations by introduction of a characteristic velocity as shown in the Appendix. These two cases are plotted in Fig. 4. Note that the aforementioned growth rates are based

7

Because the images in Fig. 2 exhibit both liquid-like and gas-like visual jet appearances, it is appropriate to also plot spreading angles for liquid sprays produced from single hole nozzles. The atomization of liquids through round single hole injectors is a complex phenomenon that depends on many parameters, including injector geometry, ambient density, viscosity and surface tension of the liquid, initial turbulence, cavitation, and liquid supply pressure oscillations. According to Reitz and Bracco[14], in the "full atomization" or simply "atomization" regime the liquid jet visually diverges immediately at the exit of the injector hole. Also, for an aerodynamic surface wave growth mechanism for liquid atomization, they show that the theoretical spray angle for a steady liquid jet can be determined by combining the radial velocity of the fastest growing unstable surface waves with the axial injection velocity. A form of an equation is then derived for the spray spreading angle that reproduces the experimental density ratio and viscosity dependency trends. They indicate that the incompressible variable density equation proposed in Abramovich[17] significantly overpredicts the spray spreading angle for all nozzles at low chamber gas densities (this equation is derived by setting the U_r to zero in equation 6 of the Appendix). This can be seen in Fig. 4. Reitz and Bracco[14] measured the spray angle in the atomization regime within the first 5 mm from the nozzle exit plane (distance-to-diameter ratios ranging from 20 to 40). Therefore, their measurements are within the comparable spatial region as the present measurements. For the two cases shown in Fig. 4, the Reynolds numbers ranged between 25,000 to 40,000. Both Reitz and Bracco[14] and Hiroyasu and Arai[28] show profound effects of the nozzle design on the spray angle. Therefore, equations proposed by Reitz and Bracco[17] for two different length-to-diameter ratios, along with their corresponding vertical error bands indicating experimental scatter around them, are shown in Fig. 4. The experimental data was for the isothermal sprays. As a cross check, a recent curve-fitted equation to experimental data proposed by Naber and Siebers[29] is also shown. They measured a transient liquid fuel jet injected into a high pressure chamber for both nonvaporizing and vaporizing sprays. The zone over which they measured their spray angles extends beyond our initial region, and this to some extent contributes to disagreement seen in Fig. 4 between the two sets of data for liquid sprays at injector length-to-diameter density ratio of about 4. Their vaporizing liquid spray data show a 15% reduction in spreading angle at a density ratio of 0.01, decreasing to no noticeable reduction at a density ratio of 0.04. This reduction is explained to be due to the contraction of the jet caused by the entrained ambient gas cooled by the vaporizing liquid, as well as the vaporization of the drops at the outer boundary of the spray. This is important and suggests that the spreading rate of the vaporizing sprays is not much different from the isothermal ones shown in Fig. 4.

In plotting the spreading rates of both liquid sprays and gas/gas turbulent mixing layers, Fig. 4 spans density ratios ranging from 0.001 to 10.0. To our knowledge, this is the first time spreading rate results have been consolidated into a single plot covering four orders of magnitude in density ratio, making this a unique and useful plot on its own. Unfortunately, the data presented in this figure does not cluster to form a universal curve. This implies that all relevant parameters are not considered in defining its axes. Clearly, within the range plotted, the constant spreading angle results for an incompressible turbulent jet overpredicts nearly all the others in Fig. 4. There is also increasing disagreement between the turbulent gas jet of Abramovich[17] and the incompressible variable density model of Papamoschou and Roshko[23] as the density ratio increases. Within the range shown, the axisymmetric jet spreading angle by Richards and Pitts[22] is higher in value than all the others. The supersonic jet angle narrows as density ratio is decreased (or Mach number increased). To some extent, disagreements in the measurements in this figure can be attributed to the different definitions of the mixing layer thicknesses, their measurement methods, and the correction factors used to convert them into equivalent visual thicknesses so they could be consolidated all in one plot, despite the fact that the best possible estimates of the conversion factors have been used. Even for those cases where the visual

Summary and conclusions

Structural transitions and the initial growth rate of jets injected into an environment at fixed supercritical temperature but at pressures varying from the subcritical to the supercritical pressure are analyzed. All evidence supports the hypothesis that the jet behaves like an incompressible but variable density gas jet when the pressure is at the critical pressure or higher. The evidence consists of: (1) the lack of any visual detection of drops in the acquired images and the visual impression of a gaseous jet; (2) the inhibition of transition into the full atomization regime as the pressure approaches and exceeds the critical pressure tested by the available atomization criteria; (3) quantitative agreement of jet growth rate measurements with theoretical equations for incompressible but variable density gaseous jets, quantitative evidence presented here for the first time; and (4) disagreement of the liquid spray growth rate data with comparable nozzle geometry to ours. Although strictly speaking droplets less than about 30 microns cannot be definitively resolved by the imaging system employed here, all the aforementioned evidence, in particular the newly demonstrated quantitative agreement between the data and previous theories, strengthens the hypothesis that supercritical jets should be treated as incompressible but variable density jets. Finally, a unique plot has for the first time been generated by converting all other types of growth rates to "visual" growth rates using the most relevant works of others on variable density incompressible mixing layers, axisymmetric incompressible and compressible gas jets, supersonic jets/mixing layers, and liquid sprays. The resulting plot of spreading angle as a function of density ratio for the first time spans four orders of magnitude in the density ratio.

Acknowledgement

20. Brown G L, and Rebollo, M R, "A small fast-response probe to measure composition of a binary gas mixture," AIAA Journal, 10, 1972, 649.

21. Abramovich, G. N., Yakovlevsky, O. V., Smirnova, I. P., Secundov, A. N., and Krasheninnkov, S., Yu. "An Investigation of turbulent jets of different gases in a general stream." Astronautica Acta, 14, 1969, 229.

22. Richards, C. D. and Pitts, W. M. "Global density effects on the self-preservation behavior of turbulent free jets," J. Fluid Mech., vol. 254, 1993, pp. 417-435.

23. Papamoschou, D. and Roshko, A.. "The compressible turbulent shear layer: an experimental study," J. Fluid Mech., vol. 197, 1988, pp. 453-477.

24. Konard, J. H. "An experimental investigation of mixing in two-dimensional turbulent shear flows with applications to diffusion-limited chemical reactions," PhD thesis, California Institute of Technology, 1976.

25. Bogdanoff, D. W. "Compressibility effects in turbulent shear layers," AIAA Journal, 21, 1983, pp. 926-927.

26. Brown, G. "The Entrainment and Large Structure in Turbulent Mixing Layers," 5th Australian Conf. on Hydraulics and Fluid Mech., 1974, pp. 352-359.

27. Dimotakis, P. E. "Two-dimensional shear-layer entrainment," AIAA Journal, 21, No. 11, 1986, pp. 1791-1796.

28. Hiroyasu, H. and Arai, M. "Fuel spray penetration and spray angle in diesel engines," Trans. JSAE, Vol. 21, 1980, pp. 5-11.

29. Naber, J. D. and Siebers, D. L. "Effects of gas density and vaporization on penetration and dispersion of diesel sprays," SAE international Congress and Exposition, SAE Paper no. 960034, Detroit, Michigan, February 26-29, 1996.

From above equations for compressible flow:

$$\frac{db}{dx} = C\frac{1+\rho_r}{2}\frac{1-U_r}{1+\rho_r U_r}; \text{ where}$$

$$U_r = \frac{U_2}{U_1} \text{ and } \rho_r = \frac{\rho_2}{\rho_1}.$$

In the main region of the jet:

$$U_r = \frac{U_{ambient}}{U_{cl}};$$

$$\rho_r = \frac{\rho_{ambient}}{\rho_{cl}}; U_{cl} = U_{cl}(x); \rho_{cl} = \rho_{cl}(x)$$

If U_r and ρ_r do not depend on x (i.e. initial region) then from above:

$$\frac{b}{x} = C\frac{1+\rho_r}{2}\frac{1-U_r}{1+\rho_r U_r} \qquad (6).$$

From experiments in the initial region
of the submerged jet (i.e. $U_r = 0$) of
an incompressible fluid ($\rho_r = 1$) $C = 0.27$
is proposed. However, various experiments
in hot jets, high - velocity jets, and
supersonic jets under off - design discharge
suggest a value of $C = 0.22$.

(b) Definition of different mixing layer thicknesses:

The vorticity thickness δ_ω is defined through measurements of the streamwise time-averaged ($\overline{U}$) velocity profile in the mixing layer. It is equal to $(U_1 - U_2)/(d\overline{U}/dy)_{max}$ where the derivative is taken across the mixing layer and U_1 and U_2 are the free stream velocities for each stream forming the mixing layer. *Brown and Roshko*[19] state that this definition, in addition to being convenient, is also appropriate, because the problem of the growth of the turbulent mixing layer is basically the kinematic problem of the unstable motion induced by the vorticity.

The Pitot thickness δ_{pit} is the width of the pressure profile measured with at Pitot tube from 5% to 95% of the difference of the two free-stream values, (see *Papamoschou and Roshko*[23]).

The visual thickness δ_{vis} is the thickness determined via a photographic technique. It is measured by the shadowgraphy and schlieren approaches in *Brown and Roshko*[19] and *Papamoschou and Roshko*[23], respectively.
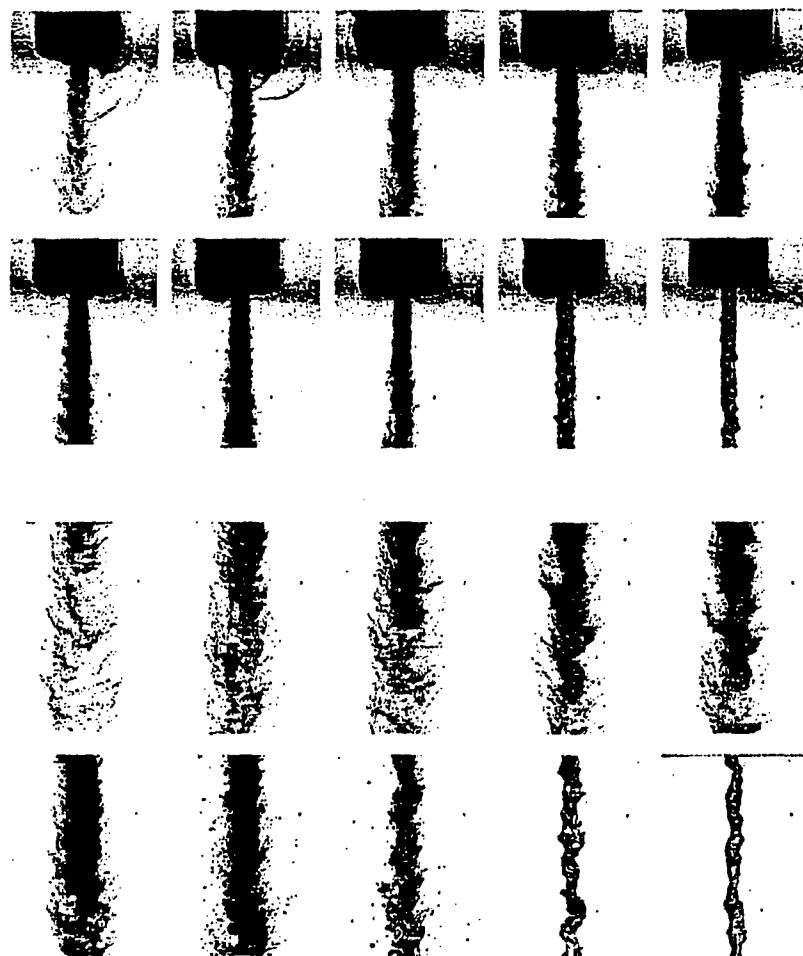
Figure 2. Back-illuminated images of the nitrogen injected into a chamber of nitrogen at a fixed supercritical temperature of 300 K but varying sub- to supercritical pressure. For the first two rows, chamber pressure decreases left to right from upper-left to lower-right corner: P_{ch}/P_c= 2.74, 2.44, 2.03, 1.64, 1.23, 1.03, 0.83, 0.63, 0.43, and 0.23. Lower two row images are corresponding images for the upper ones but further downstream. The axial distance at the bottom of the upper two row images is the same as the top of the ones in the two lower rows. The magnification can be inferred knowing the injector outer diameter of 1.59 mm (1/16"). Re # range: 25,000 to 75,000; injection velocity range: 10 to 15 m/s; Froude # range: 40,000 to 110,000. P_c and T_c are critical pressure and temperature of the injectant and P_{ch} and T_{ch} are chamber pressure and temperature. For N_2: P_c=3.4 MPa, T_c=126.2 K.

Pch=3.13 MPa
Reynolds=75,281
Mass flow=352 mg/s
Inj. Velocity=14.9 m/s

Pch=4.14 MPa
Reynolds=66,609
Mass flow=350 mg/s
Inj. Velocity=14.1 m/s

Pch=9.19 MPa
Reynolds=42,830
Mass flow=350 mg/s
Inj. Velocity=11.7 m/s

Appearance of conventional breakup of liquid surface indicating ligaments and drops ejecting from the mixing zone

Mixing layer affected by sub- to supercritical transition. No drops are seen
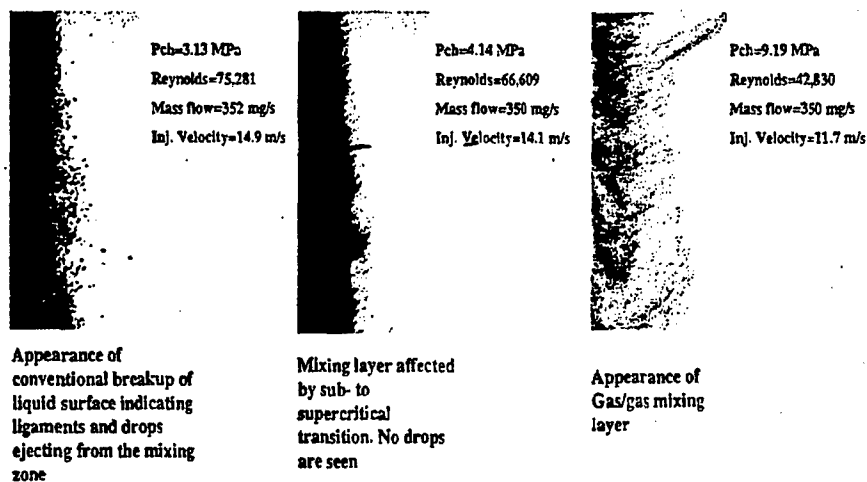
Appearance of Gas/gas mixing layer

Figure 3. Software magnified images of the jet at its outer boundary showing transition to the gas-jet like appearance starting at just below the critical pressure of the injectant. Images are at fixed supercritical chamber temperature of 300 K.

[This page is intentionally left blank.]